Uni axial compression behaviour of lightweight expanded clay aggregate concrete cylinders confined by perforated steel tube and GFRP wrapping

Sathia Ramalingam
Department of Civil Engineering, Sri Venkateswara College of Engineering
Chennai, Tamilnadu 602117 (India)
sathiamunish@gmail.com
https://orcid.org/0000-0002-0851-2145

Vijayalakshmi Ramalingam (Main and Corresponding Author)
Department of Civil Engineering, Sri Sivasubramaniya Nadar College of Engineering
Kalavakkam, Chennai, Tamilnadu 603110 (India)
vijayalakshmir@ssn.edu.in
https://orcid.org/0000-0003-4678-2020

Ramanagopal Srinivasan
Department of Civil Engineering, Sri Sivasubramaniya Nadar College of Engineering
Kalavakkam, Chennai, Tamilnadu 603110 (India)
ramanagopals@ssn.edu.in
https://orcid.org/0000-0002-5463-6616

Vikram Gopinath
Department of Civil Engineering, Sri Sivasubramaniya Nadar College of Engineering
Kalavakkam, Chennai, Tamilnadu 603110 (India)
fzvikram2504@gmail.com
https://orcid.org/0000-0003-2445-7438

Yuvarani Ramanareddy
Department of Civil Engineering, Sri Sivasubramaniya Nadar College of Engineering
Kalavakkam, Chennai, Tamilnadu 603110 (India)
yuvarani065@civil.ssn.edu.in
https://orcid.org/0000-0003-1402-6554

Yuvalatha Ramanareddy
Department of Civil Engineering, Sri Sivasubramaniya Nadar College of Engineering,
Kalavakkam, Chennai, Tamilnadu 603110 (India)
yuvalatha064@civil.ssn.edu.in
https://orcid.org/0000-0003-4516-5450

Manuscript Code: 13546
Date of Acceptance/Reception: 12.12.2020/09.05.2020
DOI: 10.7764/RDLC.19.3.200

Abstract
This study presents the experimental investigation carried out on an Expanded Clay Aggregate concrete column confined by perforated steel tube strengthened by Glass Fiber Reinforced Polymer (GFRP) sheets under uniaxial compression. Two parameters were considered for the experimental investigation: The diameter of the perforated steel tube (5 mm and 10 mm) and number of layers of GFRP wrapping (1,2, 3 and 4 layers). The compression behavior of perforated steel confined column was compared with GFRP tube encased concrete column and plain steel tube encased concrete column. The effect of perforation diameter and GFRP layers, on the failure pattern, stress-strain response, and ductility of the column were discussed. From this study, it can be concluded that the GFRP wrapping and perforated steel tube exerts the full potential to enhance the compression behaviour of expanded clay aggregate concrete column. The failure mode of GFRP wrapped perforated steel tube column was ductile in nature. The failure started with the rupture of GFRP layers followed by yielding of perforated steel tube and finally crushing of core concrete. The GFRP wrapping provides additional tensile strength to the column and the perforated steel tube with its elasto-plastic behaviour enhances the pre-cracking and post peak behaviour of the column. Better ductility performance was observed in the column with a greater number of GFRP wrapping and column with 10 mm diameter perforation.

Keywords: LECA concrete, perforated steel tube, GFRP wrapping, Confined column.

Introduction

Modern structural systems such as high-rise building, off-shore structure and bridges use Concrete-Filled Steel Tube (CFST) columns (Hajjar, 2002). In CFST column the inward buckling deformation of the steel tube is prevented by core concrete, but the steel confinement, strength and ductility are reduced by the outward local buckling. The transverse confinement outside the steel tube helps to prevent the outward local buckling of the steel tube. Such a novel form of CFST column is called confined concrete-filled steel tube columns (Xiao, 2004). Confinement to the outer steel is mainly provided by wrapping with Fiber Reinforced Polymer (FRP). FRP is widely used to strengthen the load-capacity of an element in the existing structure or it can be used in the structures during the construction itself (Teng et al., 2012). Several works were done to study the performance of FRP confined CFST column. Smith et al (2010) investigated the strength and behaviour of fiber-reinforced polymer confined concrete cylinders. Hu et al (2011) performed compressive tests on the FRP-confined concrete-filled steel tube columns, based on two parameters namely, the thickness of the steel tube and the FRP layer number. The development of local buckling deformation in the confining steel tube is substantially delayed or suppressed by the FRP wrapping.

Sundar raja & Prabhu (2012) investigated CFST columns strengthened with Carbon Fiber-Reinforced Polymer (CFRP) sheets or CFRP strips. Additional confinement pressure to the concrete core was provided by CFRP wrapping, plastic hinge formation is delayed and also constrained the local buckling of the steel tube (Feng et al., 2015; Zhang et al., 2015). Li (2007) studied the behaviour of steel-FRP tube encased concrete elements. FRP can delay the local buckling of steel tube significantly and increase the load capacity and ductility of concrete column. In addition, the FRP jacket prevents the corrosion of outer steel tube (Yu & Teng, 2013). Yan & Chou (2014) stated that, Glass Fiber Reinforced Polymer (GFRP) has higher ultimate elongation than CFRP. And also stated that GFRP is an electrical insulating material which inhibits the electrochemical corrosion with steel. But CFRP being a conductive material can induce electrochemical corrosion of steel, if the resin layer separating the steel and CFRP is compromised. Wu et al (2009) ; Wu and Jiang (2013); Huang et al (2015); Saleem et al (2019) carried out research work on GFRP wrapped CFST column. Li (2007) drilled the steel tube to form grids, this would increase the confinement efficiency and the interfacial bonding strength. Many research works have also been carried out using light weight aggregate concrete in recent years (Prakash et al., 2020; Divyah et al., 2020). Therefore, for the past two decades plain steel confined concrete columns with and without wrapping of FRP was studied in large numbers. Ans also the study of light weight aggregate concrete is also of recent interest. From the literature study it was concluded that steel confined concrete column study was carried out in an extensive manner. The behaviour of light weight concrete with perforated steel confinement is of recent interest.

Research motivation and objective of the study

Huang et al. (2016) studied the behaviour of M30 concrete cylinders confined by glass fiber reinforced polymer and perforated-steel tube subjected to uniaxial compression and compared the behaviour with GFRP wrapped concrete and steel tube encased concrete column. An interlocking mechanism is generated between perforated steel and concrete mainly due to the filling of perforation in the steel tube by fresh concrete. The transverse confinement efficiency is increased by perforated tube when compared to regular non-perforated steel tube with the same amount of steel. GFRP wrapping form a compatible deformation with steel tube, this results in increasing the ductility of the concrete column and also provided better corrosion resistance at low cost. From the literature study it can be concluded that, for the past two decades many research works have been carried out on the structure combining FRP and steel tube-encased column. But a limited information is available on the perforated steel tube encased concrete column wrapped with GFRP. Therefore, the main objective of this work is to study the stress-strain behaviour of Expanded Clay Aggregate concrete (ECA) column confined by GFRP and perforated-steel tube subjected to uniaxial compression. The compressive behavior of this hybrid structure is compared with GFRP tube encased ECA concrete and steel tube encased ECA concrete. The two parameters to be investigated in this study is the diameter of perforation in the steel tube and number of layers of GFRP wrapping. The effect of these parameters in the Stress–strain behavior, failure mode, compressive ductility is to be studied.

Experimental study

Material Properties

Ten percentage of weight of gravel was partially replaced with Expanded Clay Aggregates in the concrete mix. Four different percentage of replacement (5%, 10%, 15%, 20%) of ECA was done to study the 28 days compressive strength. Finally, 10% replacement was taken as the standard mix for the preparation of cylinder specimen. The components of

concrete were cement, sand, gravel, ECA, water, superplasticizer (BASE F). The mix proportion adopted for the materials is 1: 1.7:1.68:0.17:0.45: $8\times10^{-0.3}$. The ratio of cement: sand: gravel: ECA: water: super plasticizer. Three cubes and cylinder specimens were tested after 28 days to determine the compressive strength. After 28 days, the compressive strength of cube and cylinder specimen was 40 Mpa and 25 Mpa. Figure 1 shows the picture of ECA (Figure 1a) used in the mix and concrete specimens with different percentage of replacement of ECA (Figure 1b). The mechanical properties of the perforated steel tube were obtained by carrying out tension coupon test. Three numbers of Coupon specimens each having an average thickness of 1 mm were cut from the perforated steel tube and the test were carried out. Similarly, coupon test was carried out in GFRP sheet according to ASTM specification D3039 to obtain its material mechanical properties. The mechanical properties of perforated steel tube and GFRP sheet are listed in Table 1 and the stress strain plot is shown in Figure 2. The 5 mm and 10 mm diameter perforated steel tube before and after GFRP wrapping are shown in Figure 3.

Figure 1. Casted specimen with different percentage of replacement of ECA.

(a) Expanded Clay Aggregate (ECA) (b) Casted and cured Specimen

Table 1 Mechanical properties of steel tube and GFRP sheet

Properties	Yield Strength (Mpa)	Ultimate tensile strength (Mpa)	Modulus of Elasticity (GPa)
Perforated steel tube (D-5)	310	395	255
Perforated steel tube (D-10)	375	430	195
Stainless steel	410	450	190
GFRP tube		415	39

Figure 2. Tensile Stress strain plot of plain steel tube and perforated steel tube.

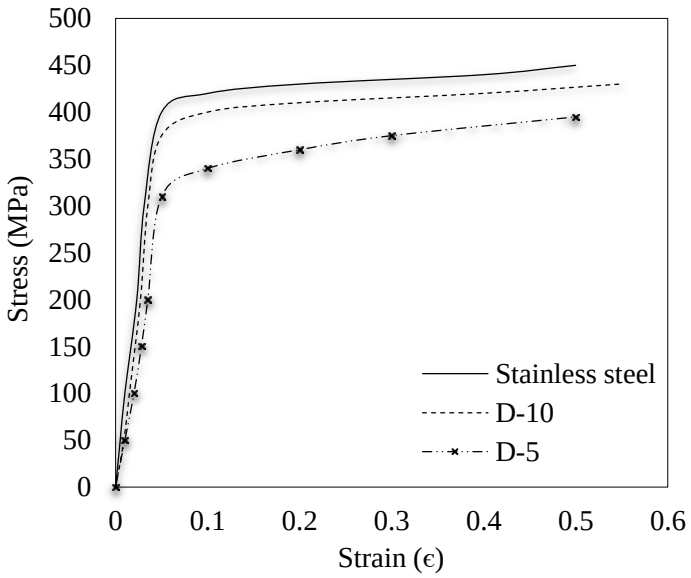

Figure 3. Perforated steel tubes (10 and 5 mm) without and with and GFRP wrapping.

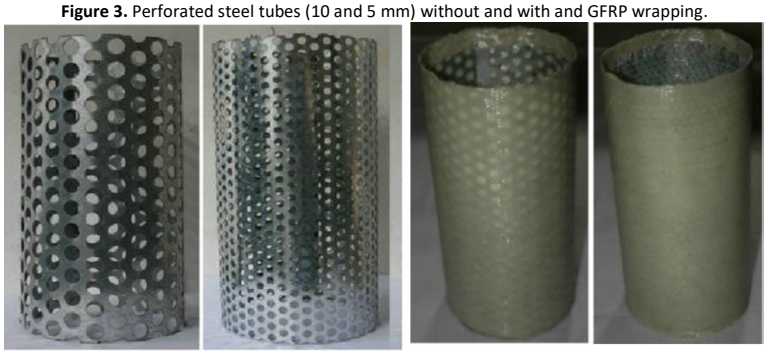

Specimen Details

Axial compression test was carried out for cylinder specimens of dimension 150 mm × 300 mm. Two experimental parameters were chosen to study the properties of GFRP wrapped perforated steel tube encased ECA concrete specimen. Steel tubes having perforation of diameter 5mm and 10 mm were used in the experimental study. One, two, three and four layers of GFRP wrapping was used in the study. Two specimens were casted for each parameter and totally 20 specimens were fabricated. The specimen details along with specimen ID are listed in Table 2. The specimen ID was given based on the number of layers of GFRP and diameter of perforation in the steel tube. For example, FRP 1-D10-ECA represent GFRP wrapping of one layer with 10 mm diameter hole in the steel tube and expanded Clay aggregate concrete. Two control specimens namely GFRP tube encased ECA concrete cylinder (GFRP-ECA) and Plain steel tube encased ECA concrete cylinders (CFST-ECA) were used for comparison. The details of the cylinder specimen with perforated steel tube and GFRP wrapping along with the control specimen is shown in Figure 4.

Table 2. Specimen details.

Specimen ID	Dimension	Number of GFRP layers	Diameter of perforation (mm)	Type of specimen
GFRP-ECA	150 × 300	-	-	Control
CFST-ECA	150 × 300	-	-	Control
FRP1-D5-ECA	150 × 300	1	5	Hybrid
FRP2-D5-ECA	150 × 300	2	5	Hybrid
FRP3-D5-ECA	150 × 300	3	5	Hybrid
FRP4-D5-ECA	150 × 300	4	5	Hybrid
FRP1-D10-ECA	150 × 300	1	10	Hybrid
FRP2-D10-ECA	150 × 300	2	10	Hybrid
FRP3-D10-ECA	150 × 300	3	10	Hybrid
FRP4-D10-ECA	150 × 300	4	10	Hybrid

Figure 4. Cylinder specimen to be tested (a) GFR wrapped-perforated steel (b)CFST (c)GFRP tube.

Test setup and Instrumentation

The axial compressive load was applied to the column specimens using Universal testing machine (UTM) of capacity 2000 KN. The specimens were instrumented to measure axial strains in the stub columns and four electrical resistant

strain gauges were used at the mid-height on the outside surface of the tubes. Two displacement transducers were used to measure the axial displacement of the column specimens. Prior to testing, steel plates were placed on top of each specimen to ensure the load was applied uniformly on the column specimens. The working of the strain gauges is tested by applying small loads and after necessary adjustments initial readings were taken. The load was applied in small increment until failure occurred. The strain readings and axial shortening were recorded using a data acquisition system for every load increment. The load arrangement and instrumentation are shown in Figure 5. Testing of Hybrid and CFST-ECA specimen is shown in Figure 6.

Figure 5. Instrumentation and test setup.

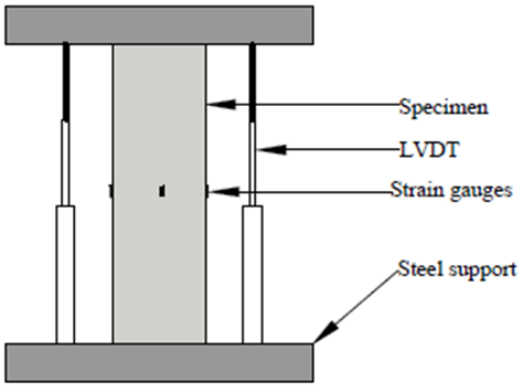

Figure 6. Testing of (a) Hybrid specimen (b) and Control specimen.

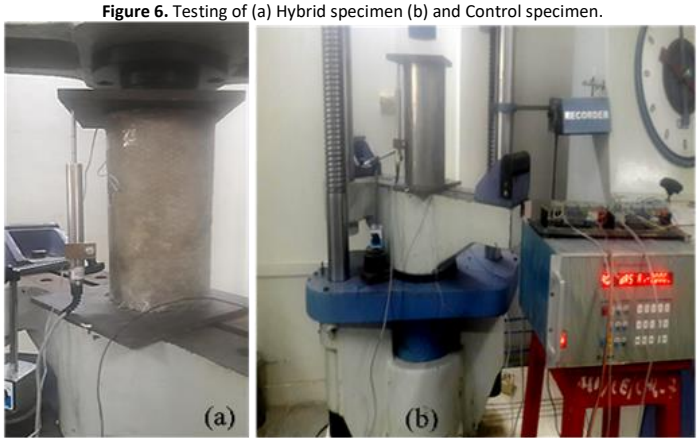

Results and discussion

Failure mode

Axial compression test was first carried out for the control specimen, which is Concrete Filled Steel Tubular (CFST) cylinder. For uniform distribution of load and to prevent end failure of steel tube, steel plate was placed on the top of the specimen. The failure started with initial bulging of the steel tube at one fourth height, followed by buckling of the steel tube. As the load increased, the inner core concrete crushed with an obvious bulging phenomenon at the final load stage. The failure pattern of CFST concrete cylinder before and after test is shown in Figure 7. After the testing of CFST cylinder, the outer steel tube was cut open to visualise the core concrete. The concrete was completely damaged with a wide crack formation (Figure 7 b).

Then, axial compression test of second control specimen i.e. GFRP tube-encased ECA concrete cylinders was conducted. During the testing, before the ultimate load capacity was achieved cracking sound of resin was heard. GFRP tube cracked suddenly with blasting sound when ultimate load was reached. The cracking of GFRP tube occurs at the middle of the cylinder. As the load increased cracking extended to both ends of cylinder and the inner core concrete was completely crushed. The failure mode of GFRP tube-encased concrete cylinder is shown in Figure 8.

Figure 7. CFST-ECA control specimen (a)before test (b) after test.

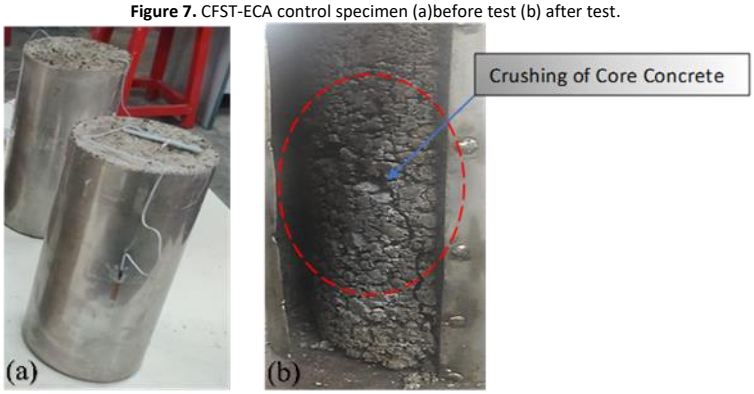

Figure 8. GFRP-ECA control specimen after test.

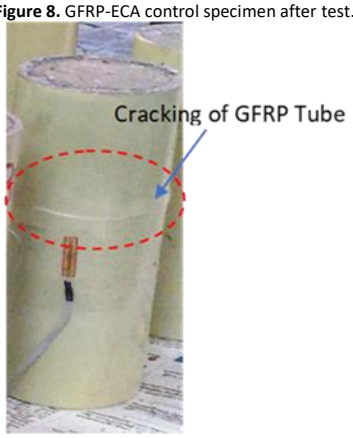

After testing the control specimen, GFRP–perforated-steel tube-encased ECA concrete cylinders were tested under axial compression. All the eight categories of specimens have different parameters such as diameter of perforation and number of GFRP layers. The diameter of perforations and GFRP layers influences the ultimate load carrying capacity of the specimen and also the post peak behaviour. On observing the failure pattern of the tested specimen, all the eight categories of specimens showed similar failure pattern. The effect of loading on the surface of the specimens was not prominent during the linear elastic stage of loading (phase 1) (Fig. 9a). As the loading increases the specimen enters the hardening state (phase 2) and failure of GFRP layers started (Fig. 9b). After the maximum load was reached (phase 3) the perforated steel tube is crushed, fractured and the GFRP layer got completely damaged with a blasting sound (Fig. 9c) and the crushing of core concrete was observed. The three-phase failure pattern of GFRP–perforated steel tube-ECA concrete cylinder is shown in Figure 9.

Figure 9. GFRP-Perforated Tube-ECA specimen (a) before testing (b) failure of GFRP sheet (c) Failure of core concrete.

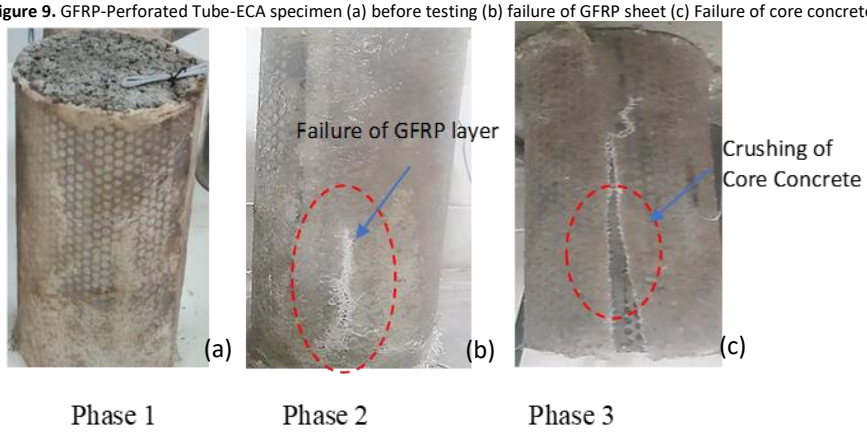

Stress Strain behaviour

The stress strain behaviour of hybrid specimen with 5 mm and 10 mm diameter perforated steel tube and 1, 2,3,4 layers of GFRP wrapping are shown in Figure 10 and Figure 11, respectively. The stress-strain graph can be divided into two parts namely the pre cracking region and post cracking region. The pre cracking region consist of linear elastic segment, where the role of GFRP wrapping and perforated steel tube have limited effect in the core concrete. The confinement provided by the outer layer does not influence the core concrete much. As the loading increases the confinement provided by the GFRP and perforated tube increases and the stress-strain region enters the post cracking region which consist of non-linear hardening stage and residual strength region (softening region).

The stress strain response of control specimen (CFST-ECA and GFST-ECA) is shown in Figure 12. The stress strain plot of CFST- ECA cylinder specimen showed that the outer steel tube provided higher confinement to the core concrete as the loading increased and the specimen enters the non-linear hardening stage. When the specimen reached its maximum load carrying capacity, the outer steel tube starts to bulge followed by failure of inner core concrete occurred. The stress strain plot showed a wide hardening region due to the confinement of plain steel to the core concrete. The residual strength region was not prominent in the CFST-ECA specimen. The stress strain plot of GFRP-ECA cylinder specimen showed that the GFRP tube provides confinement to the core concrete and as the load increases the GFRP contributes the maximum confinement and that results in a sudden rupture of the GFRP tube after the ultimate load. Therefore, the hardening region and softening region are limited in GFRP-ECA specimen. On comparing the GFRP-perforated Steel tube specimen with control specimen, specimen with GFRP wrapping and perforated steel tube result in better post cracking behaviour. The perforated steel tube provides better confinement and avoid brittle failure. The specimens also have prominent hardening region which is mainly due to the confinement of GFRP-perforated steel tube and softening plateau due the layers of GFRP wrapping. Therefore, the GFRP- perforated steel specimen possess better post peak ductility and higher load carrying capacity compared to plain CFST and GFRP tube concrete. The schematic view of stress strain graph showing different phases and the maximus stress values.

Figure 10. Stress-Strain plot of GFRP-Perforated tube (5 mm dia) confined cylinder.

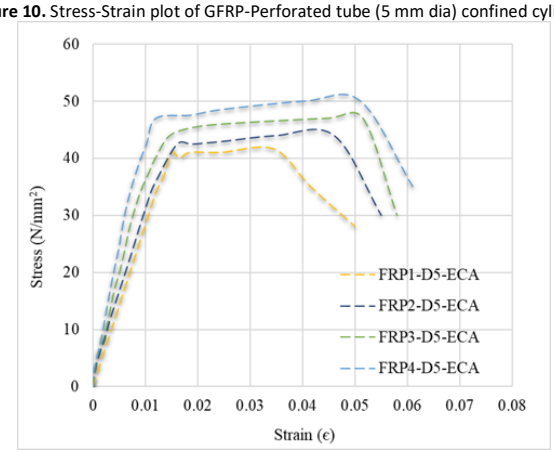

Figure 11. Stress-Strain plot of GFRP-Perforated tube (10 mm dia) confined cylinder.

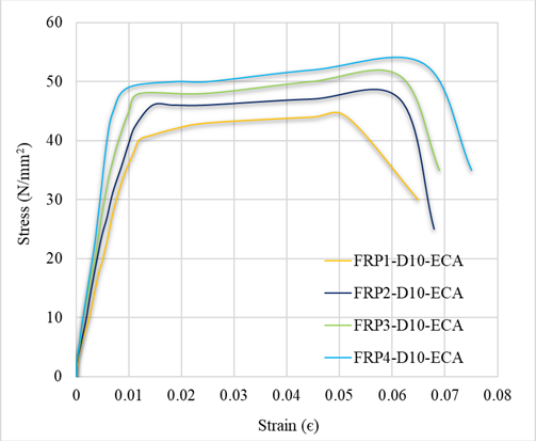

Figure 12. Stress-Strain plot of Control specimen.

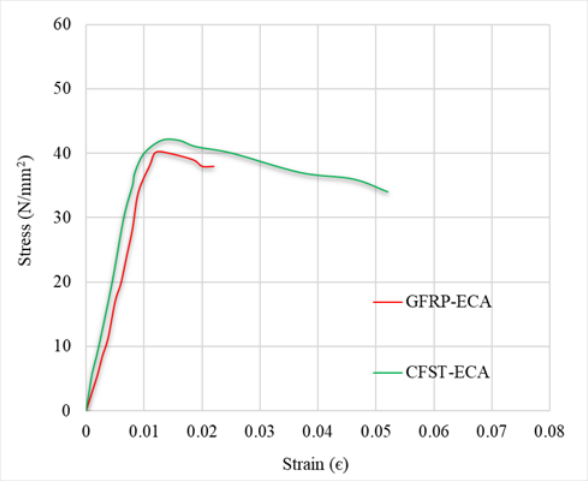

Influence of diameter of perforation

The stress strain plot of hybrid specimen with 5 mm and 10 mm diameter perforated steel tube with 1 layer of GFRP and 4 layers of GFRP is plotted for comparison and shown in Figure 13. The FRP1-D5-ECA specimen and FRP1-D10-ECA specimen showed a linear elastic portion in the beginning of load, once when the maximum elastic range is reached both the specimen showed a wide hardening region in the post peak zone. When comparing the hardening zone of D5 specimen, the D10 specimen showed a long range and moved to residual strength zone once the ultimate load is reached. From the coupon test, the yield and ultimate stress of 5 mm diameter perforated steel specimen was 310 MPa and 395 Mpa, respectively. While the yield stress and ultimate stress of D10 specimen was 375 MPa and 430 Mpa, respectively as shown in Table 1. From the above ultimate tensile stress value, it can be expected that the specimen with 10 mm diameter perforated steel tube is expected to carry more load, than specimen with 5 mm diameter perforated steel tube. From the Figure 13 the ultimate stress of FRP1-D5-ECA and FRP1-D10-ECA is 42 MPa and 44 Mpa and the ultimate stress of FRP4-D5-ECA and FRP4-D10-ECA is 50 MPa and 53 Mpa, respectively. It can be concluded that specimen with larger diameter of perforation showed higher value of ultimate load carrying capacity.

Figure 13. Stress-Strain plot to show influence of diameter of perforation of steel tube.

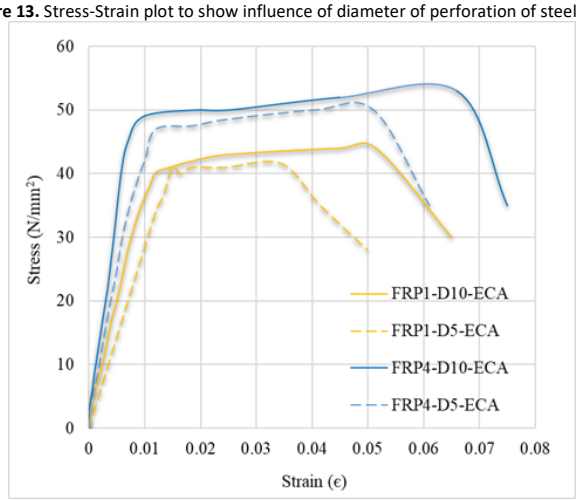

Influence of GFRP layer

The increase in number of layers of GFRP sheet has an influence in the ultimate strength of cylinder specimen. To show the effect of GFRP layer, specimen with 10 mm diameter perforated steel tube with two layer and four layers of GFRP wrapping is shown in comparison with specimen without GFRP wrapping (CFST-ECA) in Figure 14. During the initial loading stage, the stress-strain plot was observed to be linear (elastic region) for all the specimen. When comparing the specimen without GFRP wrapping (CFST-ECA), the specimens with GFRP wrapping (FRP2-D10-ECA and FRP4-D10-ECA) showed a non-linear hardening region after peak load in the elastic region was reached. The maximum ultimate stress of CFST-ECA specimen is 42 Mpa and the maximum ultimate stress of FRP2-D10-ECA and FRP4-D10-ECA 47 Mpa and 53 Mpa, respectively. The second part of stress strain curve (hardening region) is controlled by confinement of GFRP.

Therefore, as the number of Layers of GFRP increases the nonlinear curve also widens. From the study, it can be concluded that the number of GFRP layers improves the maximum load carrying capacity and also the hardening region of stress strain plot. In table 3, the stress strain values of all the ten specimens are listed.

Figure 14. Stress-Strain plot to show influence of number of layers of GFRP.

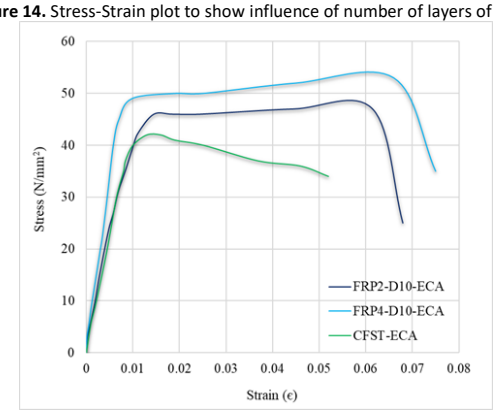

Table 3. Maximum Stress-Strain values of tested specimen.

Specimen	Maximum ultimate stress (f_{cc}) Mpa	Maximum ultimate strain (ϵ_{cc})	Stress increase with respect to GFRP-ECA (%)	Stress increase with respect to CFST-ECA (%)
GFRP-ECA	40	0.012	-	-
CFST-ECA	41	0.016	2.5	-
FRP1-D5-ECA	41.6	0.035	4	1.5
FRP2-D5-ECA	44.2	0.046	10.5	7.8
FRP3-D5-ECA	47.2	0.052	18	15.1
FRP4-D5-ECA	50.1	0.051	25.25	22.2
FRP1-D10-ECA	44	0.052	10	7.3
FRP2-D10-ECA	47	0.062	17.5	14.6
FRP3-D10-ECA	51	0.063	27.5	24.4
FRP4-D10-ECA	53	0.066	32.5	29.3

Ductility

The average ductility index of the tested specimen is obtained from three values (i) confinement ratio (ii) Confinement effectiveness and (iii) the fracture energy. The confinement ratio is the ratio of maximum strain in the confined specimen (ecc) to the maximum strain of the unconfined plain concrete cylinder (eco). Confinement effectiveness is the ratio of maximum stress in the confined specimen (fcc) to the maximum stress of the unconfined plain concrete cylinder (fco). The maximum stress and strain values of unconfined specimen are 38 Mpa and 0.004 (ϵ), respectively. The fracture energy is calculated by finding the area under the stress strain curve. The average value of confinement ratio, confinement effectiveness and fracture energy (ductility index) of different specimen is tabulated in Table 4. The ductility index value increases with the increase in number of layers of GFRP and increase in the diameter of perforation. The schematic view of stress strain graph showing different phases and the maximus stress values is shown in Figure 15.

Table 4. Measurement of ductility index.

Specimen	f_{cc} (Mpa)	ϵ_{cc}	f_{cu} (Mpa)	ϵ_{cu}	Confinement effectiveness f_{cc}/f_{co}	Confinement Ratio $\epsilon_{cc}/\epsilon_{co}$	Fracture Energy
GFRP-ECA	40	0.012	38	0.022	1.06	3	0.078
CFST-ECA	41	0.016	34	0.052	1.09	4	0.34
FRP1-D5-ECA	41.6	0.035	28	0.05	1.11	8.75	0.45
FRP2-D5-ECA	44.2	0.046	30	0.055	1.18	11.5	0.67
FRP3-D5-ECA	47.2	0.052	30	0.058	1.26	13	1.12
FRP4-D5-ECA	50.1	0.051	35	0.061	1.33	12.75	1.23
FRP1-D10-ECA	44	0.052	30	0.065	1.17	13	0.56
FRP2-D10-ECA	47	0.062	25	0.068	1.25	15.5	0.87
FRP3-D10-ECA	51	0.063	35	0.069	1.36	15.75	1.45
FRP4-D10-ECA	53	0.066	35	0.075	1.41	16.5	2.17

Figure 15. Schematics of stress strain curve showing the peak stress-strain values.

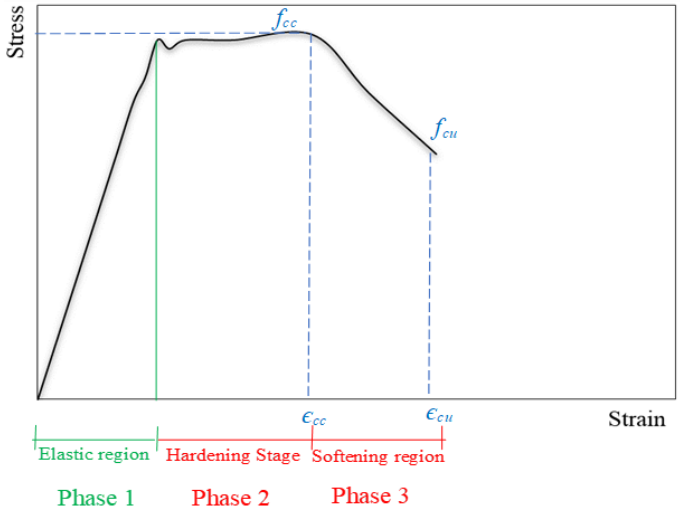

Numerical model

The design model proposed by Lam and Teng (2003) is used to obtain the stress strain values of hybrid specimen and compared it with the experimental data. According to Lam and Teng (2003) the stress strain curve is given by equ. 1 and 2:

$$\sigma_c = E_c\,\varepsilon_c - \frac{((E_c-E_2)^2)}{4f_{co}}\varepsilon_c{}^2 \qquad 0 \le \varepsilon_c \le \varepsilon_t \tag{1}$$

$$\sigma_c = f_{co} + E_2\,\varepsilon_c \qquad \varepsilon_t \le \varepsilon_c \le \varepsilon_{cc} \tag{2}$$

$$\text{Where } \varepsilon_t = \frac{2f_{co}}{E_c-E_2};\ E_2 = \frac{f_{cc}-f_{co}}{\varepsilon_{cc}}$$

The strength of confined concrete (f_{cc}) and corresponding strain (ε_{cc}) according to Richards et al (2005) is proportional to confining force as shown in equs. 3 and 4:

$$\frac{f_{cc}}{f_{co}} = 1 + k_1\left(\frac{f_l}{f_{co}}\right) \tag{3}$$

$$\frac{\varepsilon_{cc}}{\varepsilon_{co}} = 1 + k_2\left(\frac{f_l}{f_{co}}\right) \tag{4}$$

Where f_l is the lateral confinement force which is the summation of confinement force of fiber and confinement force of steel ($f_l = f_{lf} + f_{ls}$). Which is given by equs.5 and 6:

$$f_{ls} = 2\frac{f_{\theta s}t_s}{D_c} \tag{5}$$

$$f_{lf} = 2\frac{f_{\theta f}t_f}{D_c} \tag{6}$$

Where $f_{\theta s}$ and $f_{\theta f}$ are the hoop stress in steel and fibers, respectively.

t_s and t_f are the thickness of steel and fibers

D_c is the diameter of core concrete

The value of $f_{\theta s}$ suggested by Oshea and Bridge (2000) is $f_{\theta s} = \beta f_y$: where β is given by equ. 7

$$\left\{\begin{array}{ll} \beta = 1 & 0 \le c \le 0.4 \\ \beta = \frac{10(0.7-c)}{3} & 0 \ge 0.4 \end{array}\right\} \tag{7}$$

Where $c = \sqrt{\frac{f_{co}}{f_y}}$

Finally, the stress and strain equation for the hybrid specimen can be rewritten based on the above lateral confinement force. The final peak stress strain values are given by equs. 8 and 9:

$$\frac{f_{cc}}{f_{co}} = 1 + k_1\left(\frac{f_{lf}+f_{ls}}{f_{co}}\right) \quad (8)$$

$$\frac{\varepsilon_{cc}}{\varepsilon_{co}} = 2 + k_2\left(\frac{f_{lf}+f_{ls}}{f_{co}}\right) \quad (9)$$

Where K1 and K2 can be obtained from the regression analysis of the experimental results. The comparison between numerical model and experimental values are shown in Figure 16.

Figure 16. Comparison of experimental and numerical values of hybrid model.

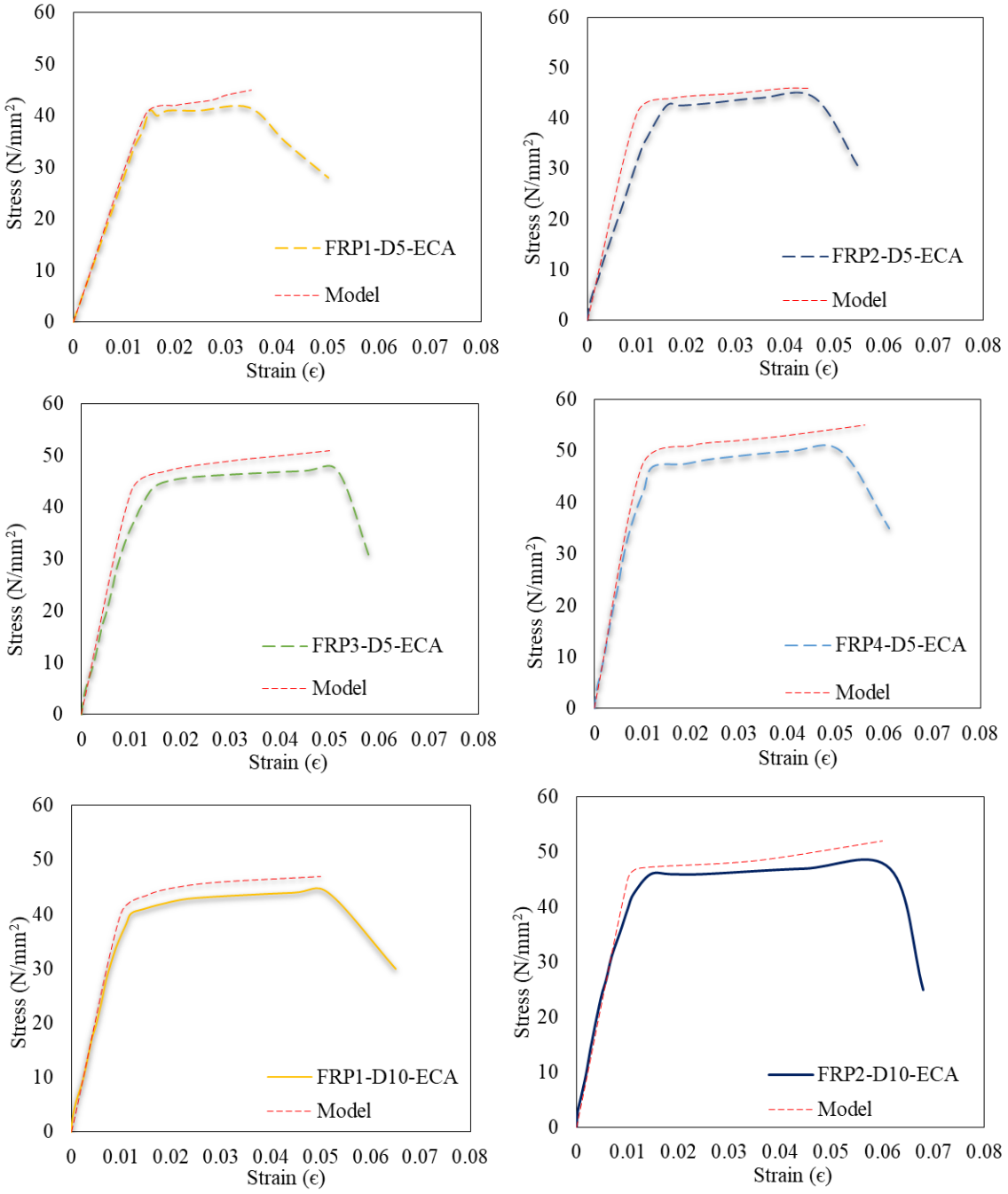

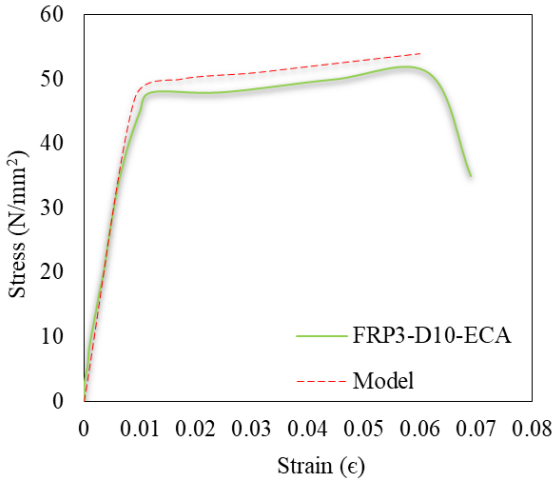

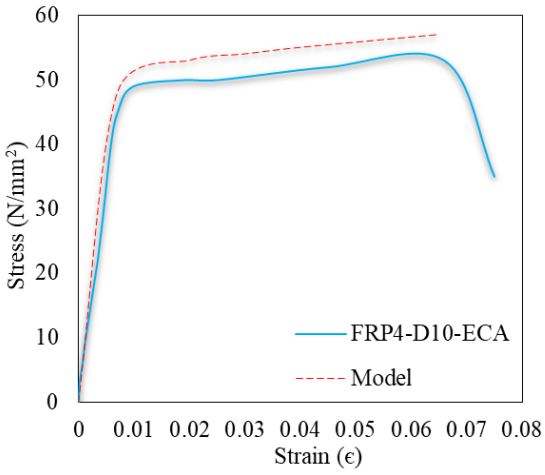

Conclusion

The following conclusion can be arrived from the compression test carried out on GFRP wrapped -perforated steel tube encased -expanded clay aggregate Concrete cylinders.

- Specimen with GFRP and perforated steel tube confinement showed ductile mode of failure. After the elastic region of curve, the failure of GFRP fibers started first, followed by buckling and fracture of perforated steel and finally the failure of core concrete occurred by bulging and crushing.
- The confinement ratio, confinement effectiveness and fracture energy which represent the ductility index is proportional to the number of layers of GFRP wrapping and diameter of perforation in steel tube. Ductility index in more for larger diameter perforated steel tube. As the number of layers of GFRP wrapping increases, the ductility index also increases.
- On comparing the GFRP-ECA specimen and CFST-ECA specimen the hybrid specimen has enhanced load carrying capacity and plastic deformation capacity. The load carrying capacity of FRP4-D10-ECA specimen, increases by 30 % and 32 % when compared to GFRP-ECA and CFST-ECA, respectively.
- The design model used to calculate the stress strain value of hybrid specimen showed good agreement with the experimental values.
- The GFRP with its high-tension strength provides maximum confinement during the hardening stage and the perforated steel with its good elasto plastic behaviour provides maximum confinement during the softening stage. Therefore, the hybrid specimen which used the advantage of both steel and GFRP is a good method of confining concrete.
- And the use of Expanded clay aggregate also has a great impact in the environment values, which can be effectively used as a replacement of natural coarse aggregate. This will also have great economic benefit without compromising the strength of concrete.

References

Divyah, N., Thenmozhi, R., & Neelamegam, M. (2020). Strength properties and durability aspects of sintered-fly-ash lightweight aggregate concrete. *Materiali in Tehnologije, 54*(3), 301–310. https://doi.org/10.17222/MIT.2019.101

Feng, P., Cheng, S., Bai, Y., & Ye, L. (2015). Mechanical behavior of concrete-filled square steel tube with FRP-confined concrete core subjected to axial compression. *Compositr Structures, 123*, 312–324. https://doi.org/10.1016/j.compstruct.2014.12.053

Hajjar, J. F. (2002). Composite steel and concrete structural systems for seismic engineering. *Journal of Constructional Steel Research, 58*, 703–723. https://doi.org/10.1016/S0143-974X(01)00093-1

Hu, Y. M., Yu, T., & Teng, J. G. (2011). FRP-Confined Circular Concrete-Filled Thin Steel Tubes under Axial Compression. *Journal of Composites for Construction, 15*(5), 850–860. https://doi.org/10.1061/(asce)cc.1943-5614.0000217

Huang, L., Sun, X., Yan, L., & Zhu, D. (2015). Compressive behavior of concrete confined with GFRP tubes and steel spirals. *Polymers, 7*(5), 851–875. https://doi.org/10.3390/polym7050851

Huang, L., Yin, P., Yan, L., & Kasal, B. (2016). Behavior of hybrid GFRP-perforated-steel tube-encased concrete column under uniaxial compression. *Composite Structures, 142*, 313–324. https://doi.org/10.1016/j.compstruct.2016.02.016

Lam, L., & Teng, J. G. (2003). Design-oriented stress-strain model for FRP-confined concrete. *Construction and Building Materials, 17*, 471–489. https://doi.org/10.1016/S0950-0618(03)00045-X

Li, G. (2007). Experimental study of hybrid composite cylinders. *Composite Structures, 78*(2), 170–181. https://doi.org/10.1016/j.compstruct.2005.08.028

O'Shea, M., & Bridge, R. (2000). Design of circular thin-walled concrete filled steel tubes. *Journal of Structural Engineering, 126*, 1295–1303.

Prakash, R., Thenmozhi, R., Raman, S. N., Subramanian, C., & Divyah, N. (2020). Mechanical characterisation of sustainable fibre-reinforced lightweight concrete incorporating waste coconut shell as coarse aggregate and sisal fibre. *International Journal of Environmental Science and Technology*, 1–16. https://doi.org/10.1007/s13762-020-02900-z

Richart, F., Brandzaeg, A., & Brown, R. L. (2005). The failure of Plain and Spirally Reinforced Concrete in Compression. *ACI Materials Journal, 10*(29), 45–52.

Saleem, M. U., Khurram, N., Amin, M. N., & Khan, K. (2019). Finite element simulation of RC beams under flexure strengthened with different layouts of externally bonded fiber reinforced polymer (FRP) sheets. *Revista de la Construccion, 17*(3), 383–400. https://doi.org/10.7764/RDLC.17.2.383

Smith, S. T., Kim, S. J., & Zhang, H. (2010). Behavior and Effectiveness of FRP Wrap in the Confinement of Large Concrete Cylinders. *Journal of Composites for Construction, 14*(5), 573–582. https://doi.org/10.1061/(asce)cc.1943-5614.0000119

Sundarraja, M. C., & Prabhu, G. G. (2012). Experimental study on CFST members strengthened by CFRP composites under compression. *Journal of Constructional Steel Research, 72*, 75–83. https://doi.org/10.1016/j.jcsr.2011.10.014

Teng, J. G., Yu, T., & Fernando, D. (2012). Strengthening of steel structures with fiber-reinforced polymer composites. *Journal of Constructional Steel Research, 78*, 131–143. https://doi.org/10.1016/j.jcsr.2012.06.011

Wu, H.-L., Wang, Y.-F., Yu, L., & Li, X.-R. (2009). Experimental and Computational Studies on High-Strength Concrete Circular Columns Confined by Aramid Fiber-Reinforced Polymer Sheets. *Journal of Composites for Construction, 13*(2), 125–134. https://doi.org/10.1061/(asce)1090-0268(2009)13:2(125)

Wu, Y.F., & Jiang, J.F. (2013). Effective strain of FRP for confined circular concrete columns. *Composit Structures, 95*, 479-491. https://doi.org/10.1016/j.compstruct.2012.08.021

Xiao, Y. (2004). Applications of FRP composites in concrete columns. *Advances in Structural Engineering, 7*(4), 335–343. https://doi.org/10.1260/1369433041653552

Yan, L., & Chouw, N. (2014). Natural FRP tube confined fibre reinforced concrete under pure axial compression: A comparison with glass/carbon FRP. In *Thin-Walled Structures, 82*, 159-169. https://doi.org/10.1016/j.tws.2014.04.013

Yu, T., & Teng, J. G. (2013). Behavior of Hybrid FRP-Concrete-Steel Double-Skin Tubular Columns with a Square Outer Tube and a Circular Inner Tube Subjected to Axial Compression. *Journal of Composites for Construction, 17*(2), 271–279. https://doi.org/10.1061/(asce)cc.1943-5614.0000331

Zhang, B., Teng, J. G., & Yu, T. (2015). Experimental behavior of hybrid FRP-concrete-steel double-skin tubular columns under combined axial compression and cyclic lateral loading. *Engineering Structures, 99*, 214-231. https://doi.org/10.1016/j.engstruct.2015.05.002